Monthly Notices
of the
ROYAL ASTRONOMICAL SOCIETY

MNRAS **443,** 411–422 (2014) doi:10.1093/mnras/stu1108

A deep and wide-field view at the IC 2944/2948 complex in Centaurus*

G. Baume,[1,2]† M. J. Rodríguez,[2] M. A. Corti,[1,3] G. Carraro[4] and J. A. Panei[1,2]

[1]*Facultad de Ciencias Astronómicas y Geofísicas – Universidad Nacional de La Plata, Paseo del Bosque S/N, La Plata (B1900FWA), Argentina*
[2]*Instituto de Astrofísica de La Plata (CONICET-UNLP), Paseo del Bosque S/N, La Plata (B1900FWA), Argentina*
[3]*Instituto Argentino de Radioastronomía (CONICET), Cno. Gral. Belgrano Km 40 (Parque Pereyra Iraola), Berazategui B1894, Argentina*
[4]*ESO, Alonso de Córdova 3107, Casilla 19001, Vitacura, Santiago de Chile, Chile*

Accepted 2014 June 3. Received 2014 June 2; in original form 2014 January 4

ABSTRACT

We employed the ESO Max Planck Institute (MPI) wide-field camera (Baade et al.) and obtained deep images in the VI_C pass-bands in the region of the IC 2944/2948 complex ($l \sim 294\overset{\circ}{.}8$; $b \sim -1\overset{\circ}{.}6$), and complemented them with literature and archival data. We used this material to derive the photometric, spectroscopic and kinematic properties of the brightest ($V < 16$) stars in the region. The *VI* deep photometry on the other end, helped us to unravel the lower main sequence of a few, possibly physical, star groups in the area. Our analysis confirmed previous suggestions that the extinction towards this line of sight follows the normal law ($R_V = 3.1$). We could recognize B-type stars spread in distance from a few hundred pc to at least 2 kpc. We found two young groups (age $\sim$ 3 Myr) located, respectively, at about 2.3 and 3.2 kpc from the Sun. They are characterized by a significant variable extinction ($E(B-V)$ ranging from 0.28 to 0.45 mag), and host a significant pre-main-sequence population. We computed the initial mass functions for these groups and obtained slopes Γ from -0.94 to -1.02 ($e_\Gamma = 0.3$) in a scale where the classical Salpeter law is -1.35. We estimated the total mass of both main stellar groups in $\sim$1100 and $\sim$500 $M_\odot$, respectively. Our kinematic analysis indicated that both groups of stars deviate from the standard rotation curve of the Milky Way, in line with literature results for this specific Galactic direction. Finally, along the same line of sight, we identified a third group of early-type stars located at $\sim$8 kpc from the Sun. This group might be located in the far side of the Sagittarius–Carina spiral arm.

Key words: stars: early-type – stars: formation – stars: pre-main-sequence – open clusters and associations: general – open clusters and associations: individual: IC 2944 – Galaxy: structure.

1 INTRODUCTION

The study of young galactic clusters and H II regions is an essential tool to improve our understanding of key astrophysical processes like star formation, its modes, spatial variation and duration (Lada & Lada 2003). At the same time, young star aggregates help us to probe the Galactic spiral structure, being one of the most prominent spiral arm tracers, together with gas, in the form of H I, H II or CO (Carraro 2014).

Our group has focused its attention in recent years to several directions in the fourth quadrant of the Milky Way – see e.g. Shorlin 1 (Carraro & Costa 2009), Danks 1 and 2 (Baume, Carraro & Momany 2009), NGC 6193/6167 (Baume et al. 2011) or CenOB1/NGC 4755 (Corti & Orellana 2013). In this paper, we extend our study to the remarkable IC 2944/2948 region, located at $l \sim 294\overset{\circ}{.}8$ and $b \sim -1\overset{\circ}{.}6$.

IC 2944 is a nebula associated with the cluster Collinder 249 (Cr 249, C1134-627, or 'λ Cen cluster') and it is centred on the star HD 101205. However, the designation IC 2944 is routinely used to identify the stellar group itself (see e.g. SIMBAD,[1] WEBDA[2]). The entire complex hosts the H II nebula IC 2948 and the stellar cluster Cr 249. The bright star λ Cen is also located in our covered field (see Fig. 1). According to Alter, Balazs & Ruprecht (1970), the entire group of brightest stars in this region is also referred as Cen OB2 association.

IC 2944/2948 appears then as a concentration of O stars (several of them identified as binary systems) and early B stars. Apparently,

*Based on observations collected at ESO La Silla, under program 076.D-0396.

† E-mail: gbaume@fcaglp.fcaglp.unlp.edu.ar

[1] http://simbad.u-strasbg.fr/simbad/
[2] http://www.univie.ac.at/webda/

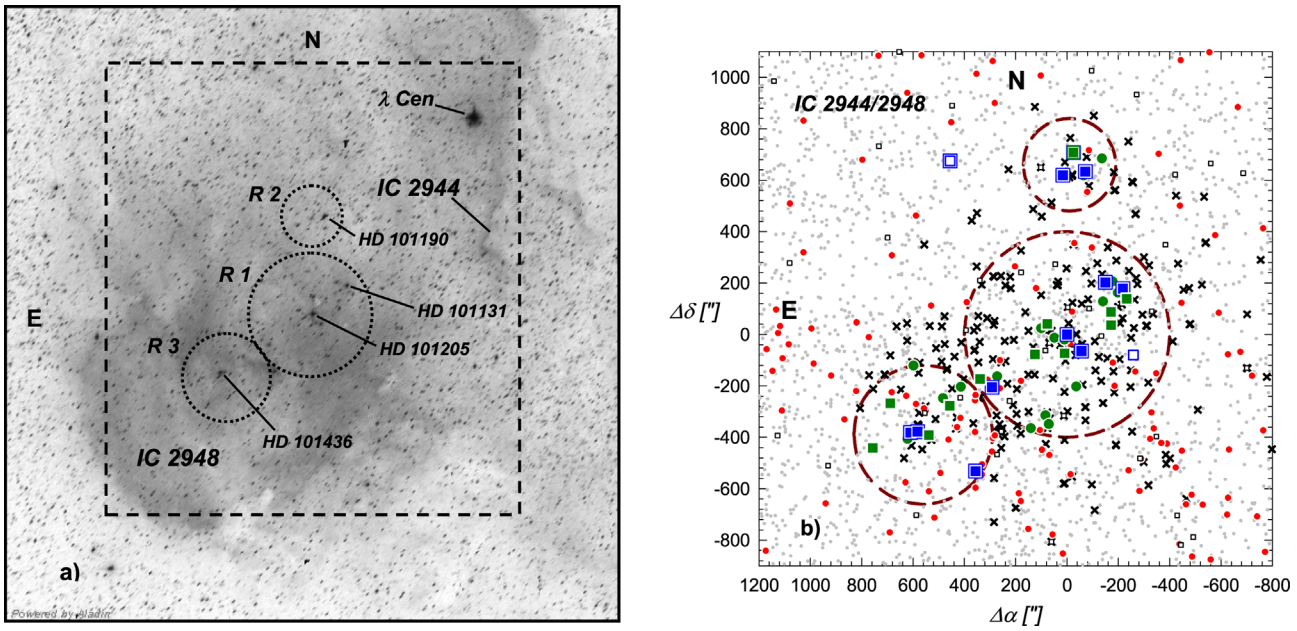

Figure 1. (a) An ALADIN-processed image from the Digitized Sky Survey. It is centred at HD 101205 ($\alpha_{J2000} = 11:38:20.4$; $\delta_{J2000} = -63:22:22.0$) and covering a field of 66.0 arcmin × 66.0 arcmin. IC 2944/2948 H II regions and main O-type stars are identified. Big dashed square indicates the full studied area covered by our VI_C data (44.6 arcmin × 48.7 arcmin) whereas the dotted circles indicate the adopted *selected regions* (see text). (b) Schematic central part of left-hand panel showing stars ($V < 21$) as symbols. Squares and circles represent stars with and without known ST classification, respectively. Filled symbols indicate stars adopted as main two groups members (see text); blue and green symbols are O and B stars, respectively. Double symbols indicate binary stars. × symbols and red dots are, respectively, X-ray sources (Nazé et al. 2013) and MSX sources (Lumsden et al. 2002) correlated with our data.

some of them are responsible for exciting the nebula. This area also contains Bok globules, which indicates the presence of an extremely young stellar population (Reipurth 2008).

The fundamental parameters of the various stellar groups have been matter of lively discussion in the literature, which prevented a general consensus on the star formation mode active in the region. Thackeray & Wesselink (1965) presented photoelectric photometry in the Johnson *UBV* system and determined radial velocities for 24 stars. They found a binary fraction greater than 50 per cent. By using these 24 objects (19 stars located within 6 arcmin of the HD 101205 star and 5 O-type stars located outside this circle), they computed the following parameters: $\overline{E(B-V)} = 0.33 \pm 0.06$, $V_0 - M_V = 11.5 \pm 0.2$ (∼2 kpc) and a mean visual absorption of 0.50 mag kpc^{-1} in this Galactic direction. On the other hand, Perry & Landolt (1986) studied several stars in this region using information in *V*, *uvby* and Hβ bands, and claimed the stars to be a mere sample of early-type field stars spread along the line of sight.

There is also poor agreement on the detailed structure of the complex, and the nature of the various apparent groups.

(i) Ardeberg & Maurice (1980, 1981) proposed that OB stars belong to various stellar groups at different distances along the line of sight. Specifically, they identify three groups: (a) the closest at about 700 pc, (b) seven bright stars that seem connected with H II region RWC62 at 1.7 kpc and (c) four more distant stars at 3–4 kpc.

(ii) Walborn (1987) suggests that the O-type stars in the field of the H II region IC 2944 constitute a physical cluster. This group of O stars is the cause of the ionization of the surrounding region.

(iii) Later, McSwain & Gies (2005) argue for the existence of a cluster, based on *b*, *y* and Hα photometry. They estimated a distance of 1.8 kpc, an age of 6.6 Myr and a reddening of $E(B-V) \sim 0.32$.

(iv) Reipurth et al. (1997) studied the globules discovered by Thackeray using CO observations and they revealed that the two larger globules are kinematically separated, and have masses of 4 and 11 $M_\odot$. However, they did not find pieces of evidence of active star formation. Accordingly, IC 2944 and IC 2948 would represent different parts of the same, large group of clouds surrounding a cluster of OB stars (Reipurth 2008).

(v) More recently, Nazé et al. (2013) studied for the first time this region using *X-ray Multi-Mirror Mission Newton* (*XMM–Newton*) data and claimed for the existence of a tight cluster.

In this paper, we perform a detailed wide-field study of the region based on *UBVIJHK* data with other complementary spectroscopic and kinematic information. We use this material to derive updated estimates of the fundamental parameters of the various stellar groups. We also analyse this field in connection with other fields located on the fourth Galactic quadrant to derive information on the spiral structure in this portion of the disc.

The layout of the paper is as follows. In Section 2, we describe the data and the reduction/calibration procedures. In Section 3, we present our analysis of the data together with several discussions. Finally, in Section 4, we summarize our conclusions.

2 DATA

This study makes use of the following material:

(i) images, in VI_C bands, obtained with the Wide Field Imager (WFI[3]) mounted at the Cassegrain focus of the MPG/ESO 2.2 m Telescope at La Silla Observatory (Chile).

[3] http://www.eso.org/sci/facilities/lasilla/instruments/wfi.html

Table 1. Journal of observations of the scientific frames together with used calibration coefficients.

Date	Frames	Exposure times (sec)× N V	I_C
08/03/2006	Short	–	10 × 9
	Long	675 × 5	675 × 5
25/04/2006	Short	10 × 9	–
	Long	675 × 5	–
28/05/2006	Short	–	–
	Long	–	675 × 10
Calibration coefficients (08/03/2006)			
$v_1 = +1.044 \pm 0.006$		$i_1 = +1.951 \pm 0.009$	
$v_2 = +0.070 \pm 0.006$		$i_2 = -0.007 \pm 0.010$	

(ii) Photometric data from the following surveys: APASS[4] (Henden et al. 2010), 2MASS[5] (Skrutskie et al. 2006) and XHIP (Anderson & Francis 2012).

(iii) Spectroscopic classification for the brightest stars from the SIMBAD and WEBDA data bases, and complemented with information from Kharchenko & Roeser (2009), Sana, James & Gosset (2011) and Sota et al. (2014).

2.1 Images

The WFI camera is a 4 × 2 mosaic of 2k × 4k CCD detectors. The scale is 0.238 arcsec pixel^{-1}, and it covers a field of view (FOV) of 34.0 arcmin × 33.0 arcmin but, due to the narrow inter-chips gaps, the filling factor of each image is ∼95.9 per cent. Images were acquired in 2006 during the nights of March 8, April 25 and May 28, and the typical full width half-maximum was in the range 0.7–1.4 arcsec, whereas air-mass values were 1.2–1.5. Details of the observations are given in Table 1.

All frames were pre-processed in the standard way using the IRAF[6] task ESOWFI/MSCRED. That is, instrumental effects were corrected with calibration images (bias and sky-flats taken during the same observing runs).

2.2 Astrometry

World Coordinate System header information of each frame was obtained using IRAF MSCZERO and MSCCMATCH tasks and UCAC4 data (Zacharias et al. 2013). This allowed us to obtain a reliable astrometric calibration. In order to go deep with our photometry, all the long exposures for each band were combined using IRAF MSCIMAGE task. This procedure helps to both removing cosmic rays and improving the signal-to-noise ratio for the faintest stars.

2.3 Photometry

Instrumental magnitudes were extracted using IRAF DAOPHOT and PHOTCAL packages, and employing the point spread function (PSF) method (Stetson 1987). Since the FOV is large, a quadratic spatially variable PSF was adopted and its calibration on each image was done using several isolated, spatially well distributed, bright stars (∼20) across the field. The PSF photometry was finally aperture corrected for each filter and exposure time. Aperture corrections were computed performing aperture photometry of the same stars used as PSF models. Finally, all resulting tables from different filters and exposures were combined using DAOMASTER (Stetson 1992) taking as reference the first night of observation (2006 March 8).

Data for stars in common with our observations (about 300) were selected from the APASS catalogue and their Sloan *gri* bands, and transformed to the VI_C system using the equations provided by Jester et al. (2005). Then, we used the following transformation equations to obtain the corresponding VI_C magnitudes from our instrumental (vi) ones:

$$v = V + v_1 + v_2(V - I_C) \quad (\mathrm{rms} = 0.05)$$
$$i = I_C + i_1 + i_2(V - I_C) \quad (\mathrm{rms} = 0.07)$$

with calibration coefficients presented in Table 1.

In order to obtain a reliable initial mass function (IMF, Section 3.7), we estimated the completeness of our optical data. The procedure was already used in our previous works (see e.g. Baume et al. 2003). Basically, we created several artificial images by adding stars in random positions on to the original images using ADDSTAR routine of DAOPHOT. The added stars were distributed in luminosity as the real sample. In order to avoid overcrowding, in each experiment, we added the equivalent to only about 15 per cent of the original amount of stars. Since V-band images are shallower than those in the I band, we have adopted for the latter the completeness factor (CF) estimated for V. The CF is defined then as the ratio between the number of artificial stars recovered and the number of artificial stars added, and our results are listed in Table 2.

2.4 Kinematic data

Radial velocity information for stars in the zone were extracted from different bibliographic sources and data bases. In detail, we obtained heliocentric radial velocities for 50 stars: 3 stars from SIMBAD data base, 19 from Kharchenko et al. (2007) and Kharchenko & Roeser (2009), 20 from Huang & Gies (2006), 4 from Thackeray & Wesselink (1965), 1 from Conti, Leep & Lorre (1977), 1 from Gies et al. (2002) and 2 stars from Sana et al. (2011). Regarding proper motions, all data were extracted from the UCAC4 catalogue.

2.5 Mid-IR and X-ray data

We cross-correlated our photometric data with mid-IR and X-ray data with the purpose of detecting pre-main-sequence (PMS) stars (see also Section 3.2.2).

As for the mid-IR data, we use The Midcourse Space Experiment (MSX) data (Egan et al. 2003). MSX mapped the Galactic plane and other regions missed or identified as particularly of interest by the *Infrared Astronomical Satellite* at wavelengths of 4.29, 4.35, 8.28, 12.13, 14.65 and 21.3 μm.

The Nazé et al. (2013) catalogue was used for the X-ray data. These data were obtained using the *XMM–Newton* information. These data resulted by binning their three energy bands: soft = S = 0.3–1.0 keV, medium = M = 1.0–2.0 keV and hard = H = 2.0–10.0 keV.

These data were cross-correlated with our optical data using ALADIN[7] tool. To this aim, we use a 3.0 arcsec search radius for the *XMM* data, and a 10.0 arcsec radius for the MSX data – see

[4] http://www.aavso.org/apass

[5] http://irsa.ipac.caltech.edu/Missions/2mass.html

[6] IRAF is distributed by NOAO, which is operated by AURA under cooperative agreement with the NSF.

[7] http://aladin.u-strasbg.fr/

Table 2. CFs of optical data.

V	14–15	15–16	16–17	17–18	18–19	19–20	20–21	21–22	22–23	23–24
CF (per cent)	100	100	100	100	98	95	92	81	76	23

Lumsden et al. (2002) and Nazé et al. (2013). We used the *all matches* option in ALADIN since this option gave us all the counterparts within the searching radius. Following these criteria, we found 139 counterparts in X-ray and 73 in mid-IR.

2.6 Final catalogue

We used the STILTS[8] tool to manipulate tables and we cross-correlated our VI_C data with the other public *UBVIJHK* photometry and the available spectral classification. In this process, we adopted ESO/WFI VI_C data only for objects with $V > 13$. We obtained then a catalogue with astrometric/photometric information of about 130 000 objects covering approximately an FOV of 44.6 arcmin × 48.7 arcmin around IC 2944/2948 (see Fig. 1). A more reliable analysis of the behaviour of the stellar energy distributions could be carried out with such a catalogue (at least for brightest stars), thus preventing possible degeneracies in the photometric diagrams. The full catalogue is available in electronic form at Centre de Données astronomiques de Strasbourg (CDS) website (http://cdsweb.u-strasbg.fr/cgi-bin/qcat?J/MNRAS/).

3 ANALYSIS AND DISCUSSION

3.1 Selected regions

We started our study by identifying three regions where a visual overdensity of early-type stars could be detected. These regions are shown as dotted circles in Fig. 1 and they are defined as follows:

(i) *Region 1 (R1)*: a circle centred at $\Delta\alpha = 0.0$ arcsec, $\Delta\delta = 0.0$ arcsec and radius 400.0 arcsec
(ii) *Region 2 (R2)*: a circle centred at $\Delta\alpha = -10.0$ arcsec, $\Delta\delta = +660.0$ arcsec and radius 180.0 arcsec
(iii) *Region 3 (R3)*: a circle centred at $\Delta\alpha = 560.0$ arcsec, $\Delta\delta = -390.0$ arcsec and radius 270.0 arcsec,

where we have used a coordinate system centred on HD 101205 star ($\Delta\alpha = (\alpha - \alpha_{\rm HD101205})\cos(\delta_{\rm HD101205})$; $\Delta\delta = \delta - \delta_{\rm HD101205}$).

3.2 Spectrophotometric study

3.2.1 Upper main sequence

Our compilation of spectroscopic data allowed us to estimate the distance and colour excess of 162 stars located in our FOV. We applied then the traditional method (e.g. Corti, Arnal & Orellana 2012) based on the absolute magnitude M_V and intrinsic colours calibration provided by Martins & Plez (2006) for O-type stars and by Schmidt-Kaler (1982) for B and later ones. We adopted an M_V uncertainty of 0.5 mag (Walborn 1972) and a value $R_V = A_V/E(B-V) = 3.1$ (see in advance Fig. 3 b). A linear interpolation was performed in case of missing spectral type (ST) calibration. In order to reduce the uncertainty, for binary systems, where both stars were classified (SB2), we obtained distance and colour excesses by computing first the individual component magnitudes/colours and then we applied the above method. For binary systems with only one classification (SB1), we assumed that our results have an additional minor uncertainty.

Computed distances and colour excesses for known OB stars led us to the distributions presented in Fig. 2, where we noticed the following features.

(i) Stellar densities (see scale on right axis) indicate a high concentration of young stars located in the selected regions in relation with the field values, confirming the criteria used in their choice.
(ii) Regarding the colour excesses, the three regions are suffering some differential reddening; however, it was possible to distinguish a concentration of values on each one. In, particularly, $R1$ and $R2$ this concentration is around $E(B-V) = 0.33$ and in $R3$ it is around $E(B-V) = 0.43$. On the other hand, field stars reveals a wide spread of values with one O-type star with a strong reddening ($E(B-V) \sim 1$).
(iii) Distance distributions reveal a clear peak in $R1$ and $R2$ at $V_0 - M_V = 11.8$ and this value could be adopted also as a representative value for a possible stellar group ('a') placed in these regions. In $R3$, $V_0 - M_V = 12.5$ appears as a better representative value for another possible stellar group ('b'). Additionally, there is one B-type star at about $V_0 - M_V = 9.25$ located in $R1$, and there are two O-type stars at about $V_0 - M_V = 14$, one of them in $R1$ and the other in the field. These later two stars could be part of another group of young stars ('c'). There is also a set of B stars covering an important range in distance, from a few hundred pc to at least 1.5–2 kpc with an average stellar density ∼60 per cent higher than the average in the solar neighbourhood (Allen 1973).

All these facts are reflected in the two-colour (TCDs) and colour–magnitude diagrams (CMDs) shown in Figs 3 and 4, respectively. In particular, Fig. 3(a) reveals the already-indicated differential reddening with excess values ranging from 0.28 to 0.45, and Figs 3(b) and (c) indicate no evident deviations from the normal reddening law ($R = A_V/E(B-V) = 3.1$) in the zone, in agreement with previous polarimetric studies (see Vega, Orsatti & Marraco 1994).

3.2.2 Lower main sequence

To study the lower main sequence (MS) ($V > 14$), we first attempt to quantify field-star contamination. To this purpose, we developed a code that performed a statistical decontamination of the field stars over the CMDs (see Gallart et al. 2003). Briefly, the procedure consists in a star-by-star position comparison on to the CMDs of each region ($R1$, $R2$ and $R3$) and a CMD of a representative field located near them and covering the same sky area. Then, we subtract field stars with similar position (colour and magnitude) from the CMDs to obtain a decontaminated diagram. For this task, we used our V versus $V - I$ diagrams since they are the deepest ones. In Fig. 5, we present the resulting CMDs, where we could identify a highly probable PMS population (small red circles). To strengthen our results, we use X-ray data as additional membership criteria.

[8] http://www.star.bris.ac.uk/mbt/stilts/

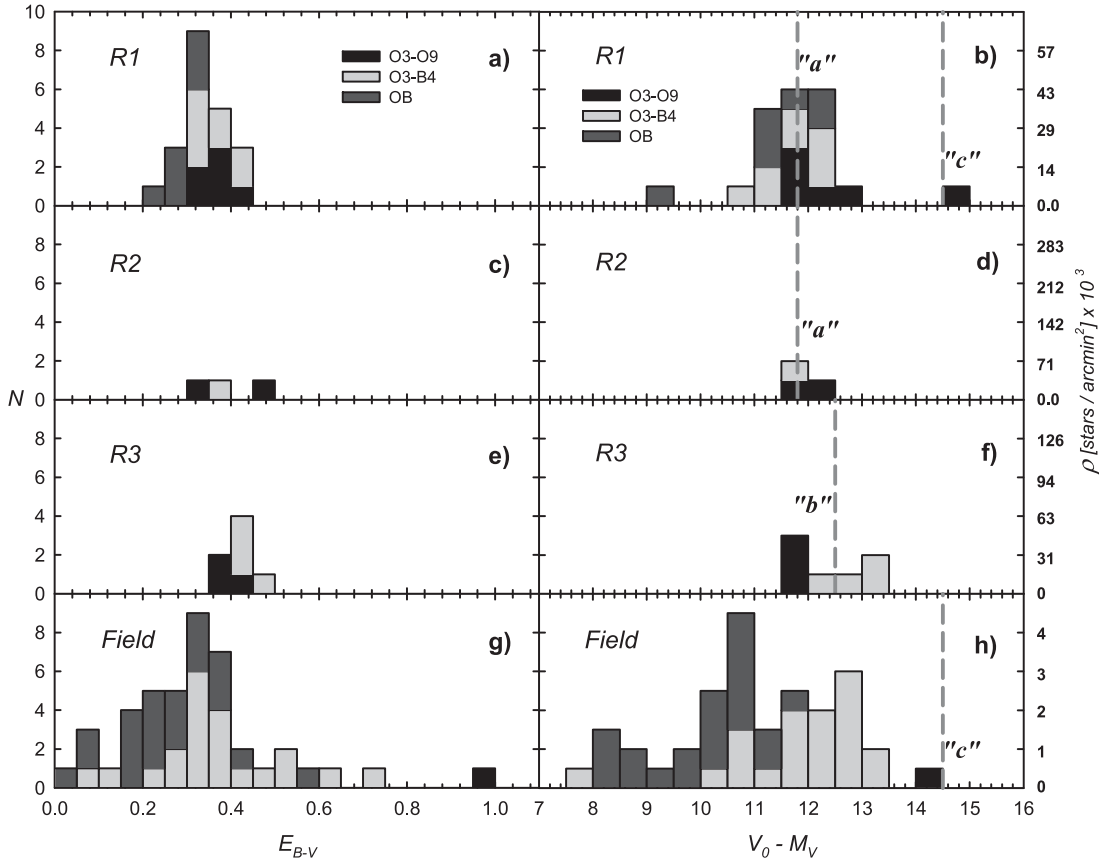

Figure 2. Distributions of the $E(B-V)$ and spectrophotometric $V_0 - M_V$ of OB stars with known ST and located inside the selected regions (see Fig. 1). Dashed lines in right-hand panels indicate adopted $V_0 - M_V$ values for stellar groups/populations placed in each region. For a better understanding, the highest bar of panel (a) means: two O3–O9 stars, six O3–B4 stars and nine OB stars.

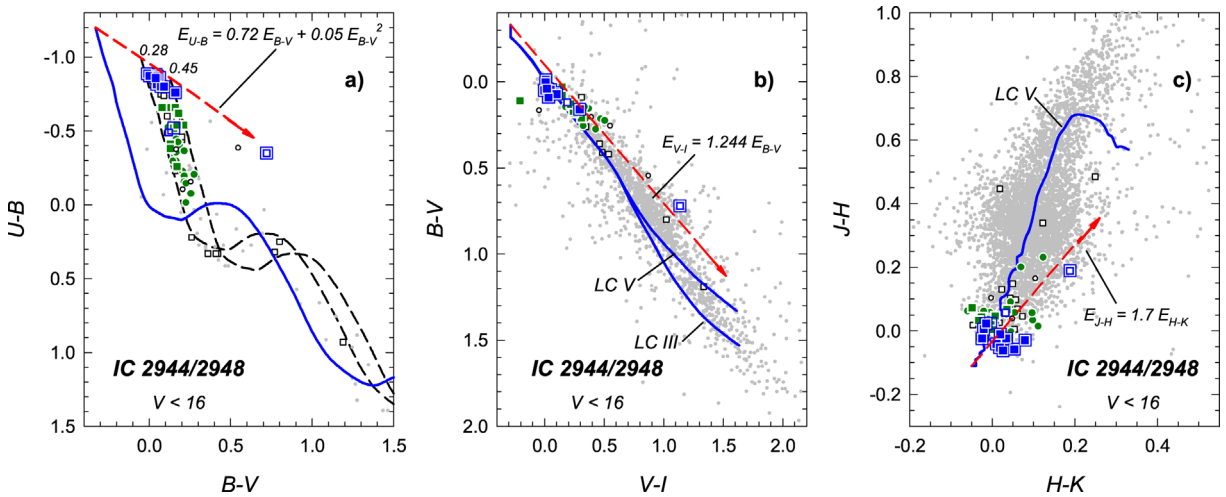

Figure 3. TCDs for the brightest stars ($V < 16$) in our sample. Symbols are as in Fig. 1(b). The solid (blue) curve in plot (a) is the Schmidt-Kaler (1982) ZAMS, while dashed (black) curves are the same ZAMS, but shifted along the reddening line (red) by the colour excesses indicated above them. Solid (blue) curves in plot (b) are intrinsic colours for luminosity class V and III from Cousins (1978a,b). Solid (blue) curve in plot (c) are intrinsic colours for luminosity class V from Koornneef (1983). Dashed (red) arrows indicate the normal reddening path ($R_V = 3.1$).

PMS stars are routinely identified using X-ray emission and this kind of observations should reveal almost all (∼90 per cent) the PMS population up to the corresponding detection limit (Feigelson & Getman 2005). Different panels in Fig. 5 (×symbols) reveal their spatial distribution over the three selected regions. We also cross-correlated our data with IR sources present inside these three regions (big grey circles in Fig. 5). In particular, we mark those ones (red triangles) with infrared behaviour expected for young stellar objects (YSOs), say with an infrared rising energy distribution – $F_{21}/F_{14} > 1$ and $F_{14}/F_8 > 1$ (Lumsden et al. 2002).

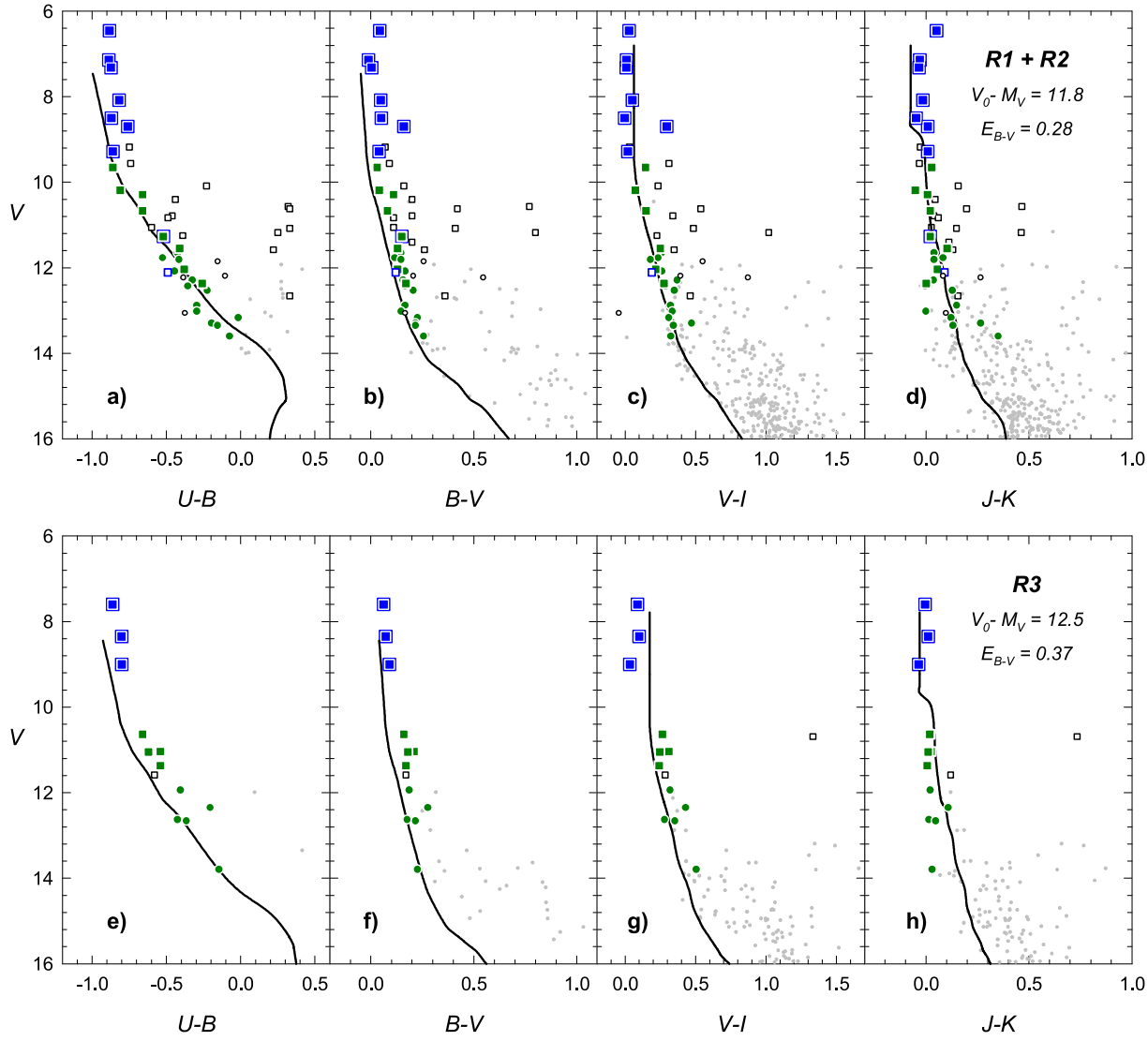

Figure 4. CMDs of stars placed in the three selected regions of the studied zone (see Fig. 1b). Symbols have the same meaning as in that figure. Solid (black) curves are the Schmidt-Kaler (1982) ZAMS (for *UBV*), the Cousins (1978a,b) MS (for *VI*) and the Koornneef (1983) MS (for *JHK*) corrected by the respective adopted colour excesses and apparent distance moduli for each stellar group located in each region (see Table 3).

We could remark the following: (a) most optical sources that could be associated with an X-ray counterpart follow closely the colour and magnitude distribution of the stars we selected as probable PMS objects after the field-star decontamination. (b) The observed width in both sets of data could be caused by an age spread, binary stars, accretion stellar discs – Preibisch & Zinnecker (1999) and Kenyon & Hartmann (1990) – or/and differential reddening. (c) The amount of X-ray sources is significantly lower than those revealed in the decontamination process and (d) We found only a few probable YSOs (Fig. 5c).

3.3 Stellar groups and selected stars

The analysis in Section 3.2.1 allowed us to better understand this particular Galactic direction. Previous work by other authors (see Section 1) claimed the presence of a spread of early stars along the line of sight or the presence of several stellar groups. Our analysis indicated that we could recognize a spread of early (B-type) star, two main stellar groups and a young background stellar population. Each group exhibits an important dispersion in distance/excesses, which one can explain with spectroscopic errors, and other well-known effects such as multiplicity, evolution, fast rotation and/or differential reddening. The main stellar groups/populations can be described as follows.

(i) 'a': this stellar group is located at about 2.3 kpc from the Sun, suffering an $E(B-V)$ ranging from 0.28 to 0.40, and mainly located in *R*1. However, the brightest stars of *R*2 revealed similar properties and they were also considered part of the same stellar group.

(ii) 'b': this stellar group is at about 3.2 kpc from the Sun, suffering an $E(B-V)$ ranging from 0.37 to 0.45, and mainly located in *R*3.

(iii) 'c': this is an apparent spread of young background population at about 8 kpc from the Sun, represented in our data by at least two O-type stars.

Under these assumptions and adopting a normal reddening law, we simultaneously fit a zero-age main sequence (ZAMS) or an

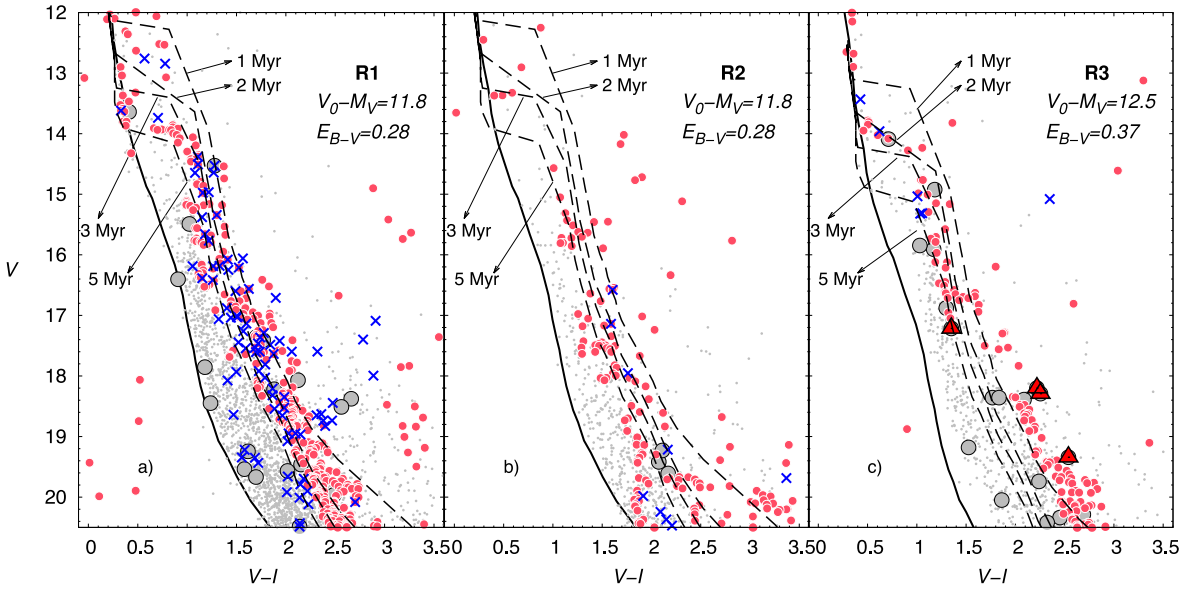

Figure 5. Detailed CMDs of stars located in the three selected regions (grey dots). Solid curves are the Schmidt-Kaler (1982) and Cousins (1978a,b) empirical MS; dashed curves are Siess, Dufour & Forestini (2000) isochrones for $z = 0.02$. All the reference curves are corrected by the adopted colour excesses values and apparent distance moduli (see Table 3). Red circles are stars resulting from statistical subtraction between each selected region and a comparison region. Blue '×' are optical sources correlated with X-ray sources. Big circles are optical sources correlated with MSX ray ones and red triangles are considered YSOs.

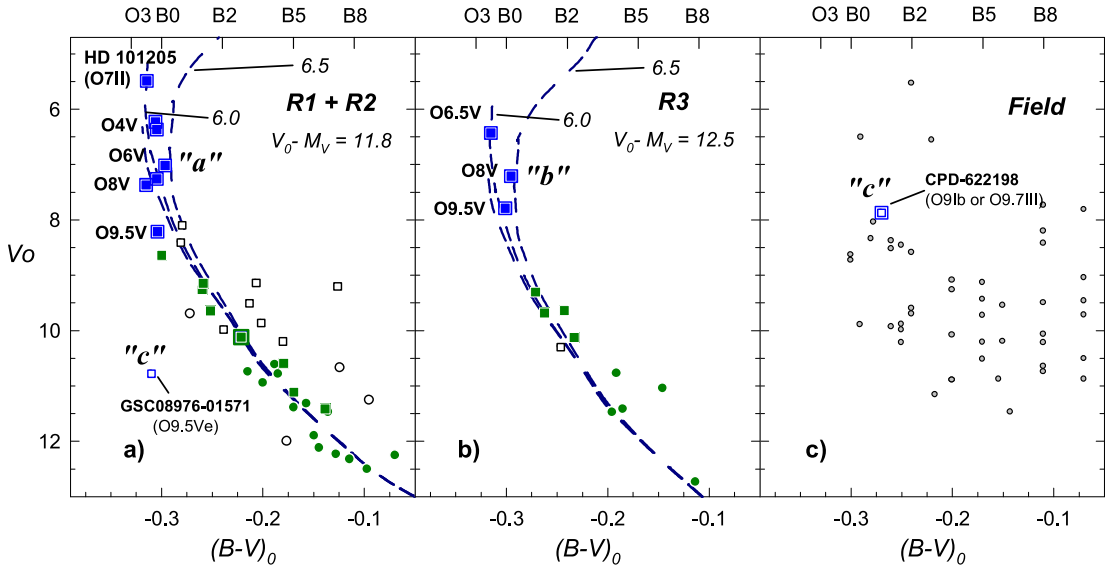

Figure 6. Corrected CMDs of stars presented in Fig. 4. Symbols are as in Fig. 1(b). Dashed (blue) curves are Marigo et al. (2008) isochrones for $z = 0.02$ (numbers indicates log(age[yr])). All the reference curves are corrected by the respective adopted distance modulus (see Table 3). Upper axis indicates ST for MS stars. O stars representative of each stellar group/population are indicated with letters 'a', 'b' and 'c'.

MS in all the CMDs (see Fig. 4) at respective main groups distances revealed in Fig. 2. These relationships closely follow both the brightest stars and the fainter B-type ones.

In Fig. 6, we present the corrected CMDs for brightest ($V < 14$) stars located in $R1 + R2$, $R3$ and the field around them in different panels. We use only stars with available ST classification, or for which it was possible to apply the classic de-reddening method (see Baume et al. 2003) and the relation $E(U - B)/E(B - V) = 0.72 + 0.05E(B - V)$ (see Fig. 3a). We noticed that in Fig. 6 stars located in $R1 + R2$ and $R3$ show consistent magnitude and spectral classification sequences and it seems conceivable to associate most OB stars in each panel with the stellar groups 'a′ and 'b′ mentioned above.

A few stars deserve additional comments (see also Fig. 6):

(i) HD 101205: it is the brightest star in the selected regions and is classified at SIMBAD as an O8 V but as an O7 II by Sota et al. (2014). In both cases, this star does not follow the above-indicated sequence and under the former classification it yields an spectroscopic $V_0 - M_V = 10.2$. However, adopting the later classification and considering that it is a quadruple system with at least three OB components (Sana et al. 2011), it is possible to

Table 3. Parameters of main stellar groups.

Parameter	'a'	'b'	'c'
$V_0 - M_V$	11.8 ± 0.2	12.5 ± 0.2	$\sim$14
$E(B-V)$	0.28–0.40	0.37–0.45	$\sim$1?
Nuclearage (Myr)	$\sim$3	$\sim$3	$\sim$10?
Contractionage (Myr)	$\sim$3–5	$\sim$2–3	–
IMFslope (Γ) (case a)	-1.00 ± 0.35	-1.02 ± 0.37	–
(case b)	-0.94 ± 0.27	–	–
Totalmass ($M_\odot$) (case a)	$\sim 1100 \pm 200$	$\sim 470 \pm 100$	–
(case b)	$\sim 1200 \pm 200$	–	–
Kinematic values from O member stars			
$\mu_\alpha \cos(\delta)$ (mas yr^{-1})	$-5.1 \pm 1.2(7)$	$-6.1 \pm 1.1(2)*$	$\sim -0.2?(2)$
μ_δ (mas yr^{-1})	$+0.2 \pm 1.2(7)$	$-0.7 \pm 0.8(2)*$	$\sim -5.6?(2)$
RV_{LSR} (km s^{-1})	$+5.9 \pm 2.8(5)**$	$+4.4 \pm 0.5(2)$	$\sim -10.7?(1)$

Notes. Number of stars is indicated in parenthesis.
*Star HD 101436 is excluded.
**Stars HD 101205 and HD 101223 are excluded.
IMF case a: HD 101205 star was not considered as member.
IMF case b: HD 101205 star was considered as member.
?: very uncertain values

explain its particular location on Fig. 6 and could be considered as a group 'a′ member.

(ii) CPD-62°2198: this star is placed among other well-located MS O-type stars but it is located in the field, outside the selected regions *R*1, *R*2 and *R*3. This star is classified as a supergiant (O9 Ib; WEBDA) or as a giant (O9.7 III; Sana et al. 2011), revealing that it could have a spectroscopic distance moduli of 14.2 or 13.0, respectively. In any case, this star would be behind the main stellar groups and it would be part of the so-called population 'c'.

(iii) HD 101333: this star is also located along an MS (see Fig. 6); however, it is classified as a giant (O9.5 III; SIMBAD) or a dwarf (O9.5 V; Sana et al. 2011). In the former classification, it would share the place with CPD-62°2198, but, if a dwarf, it could still be considered part of the 'b' group.

(iv) HD 308804: this star has also different ST classifications. It is an O9.5 Vn in SIMBAD and a B3 V by Sana et al. (2011). As an O-type star, it would have a similar distance as CPD-62°2198. However, by adopting the later ST, it could be considered member of the 'a' group.

(v) GSC08976-01571: this star is classified as an O9.5 Ve (WEBDA). It is placed in *R*1 but it is a too faint MS star to belong to the main stellar groups. With a spectroscopic distance $V_0 - M_V = 14.8$, it could be a member of the 'c′ group.

The resulting parameters of the main stellar groups and background stellar population are summarized in Table 3.

3.4 The Galactic spiral structure

Previous investigations – Carraro & Costa (2009), Baume et al. (2009, 2011) and references therein – presented their analysis of optical observations along directions close to the field studied in this paper. In all cases, several early-type star groups (usually three) were detected along the line of sight, and they were considered as belonging to spiral features located at increasing distance from the Sun.

In this work, we found several populations of young stars as well, thus lending further support to our earlier results. In this study, we found: (a) a population represented by several B-type stars scattered form a few hundred of parsecs to at least 1.5–2 kpc of the Sun; (b) a second population identified by the young stellar groups 'a' and 'b' with several O stars situated at 2.3 and 3.2 kpc, respectively and (c) a third population which is represented by at least two O stars (one in *R*1 and other in the field) identified as population 'c' and located at about 8 kpc.

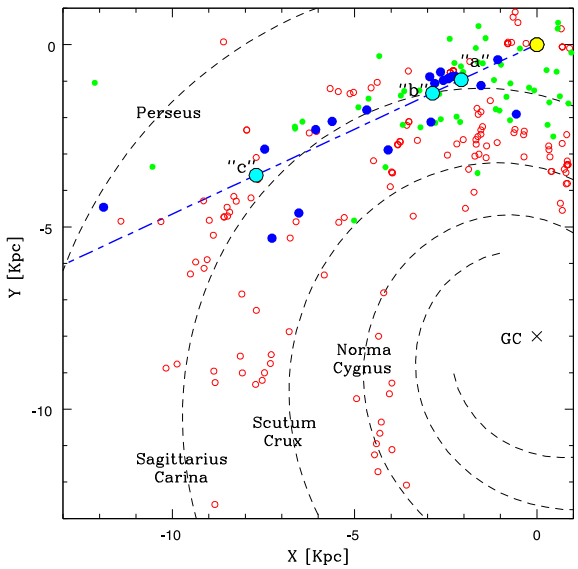

Figure 7. Comparison of the studied Galactic direction (dashed blue line) to the Vallée (2008) model with four arms. The big cyan open circles indicate the studied 'a' and 'b' stellar groups and the background young stellar population 'c' (see Section 3.3). We assumed a distance to the Galactic Centre of $R_0 = 8.0$ kpc. Other stellar populations are plotted for reference: (green) points are Cepheid (Majaess, Turner & Lane 2009); filled (blue) circles are open clusters and young groups from optical (*UBVI*) data (from several studies) and open small (red) circles mark the H II tracers (Hou, Han & Shi 2009). The yellow circle marks the position of the Sun.

The results of this paper together with previous results are presented in Fig. 7 where the Vallée (2008) spiral arms' model is also shown as dotted curves. It reveals then a consistent picture between the described groups/populations and those already known. It seems necessary to study more directions close to this region using optical

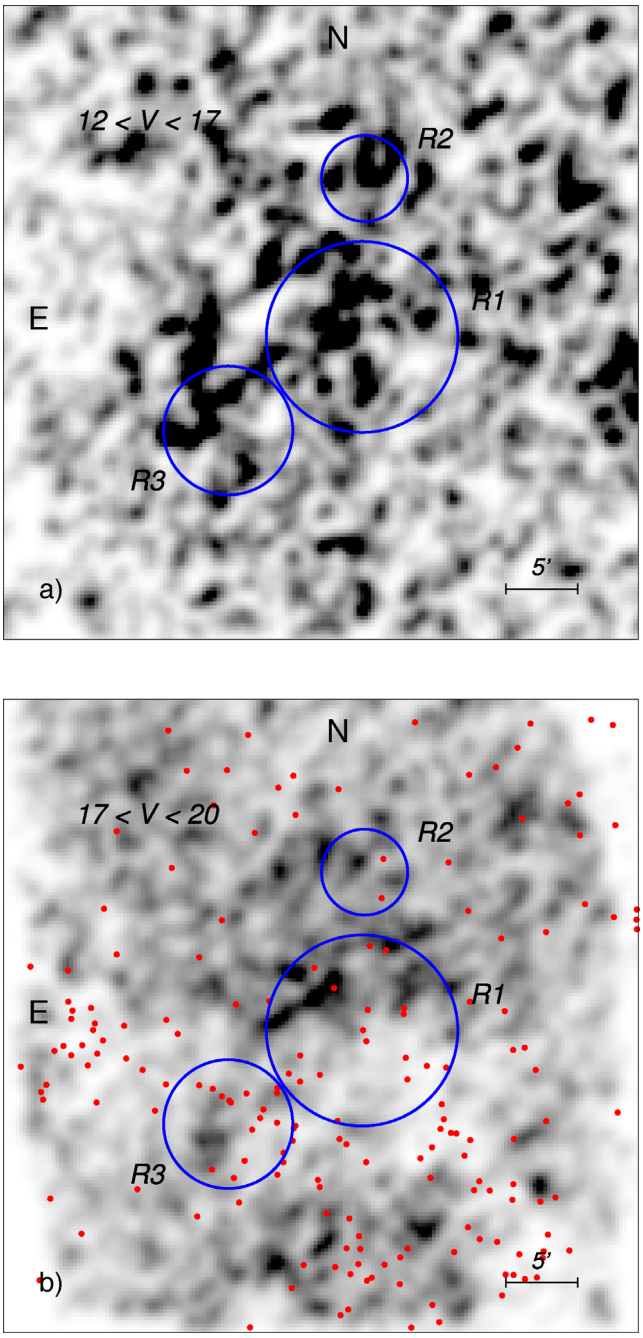

Figure 8. Density maps for stars located between two PMS isochrones (see text). Both panels discriminate stars brighter and fainter than $V = 17$. Blue circles indicate the selected regions. Red dots are MSX sources (Lumsden et al. 2002) correlated with our optical data.

and infrared observations of young objects to complete the picture of spiral structure in the fourth Galactic quadrant.

3.5 Dating the stellar groups

In order to estimate the ages of the main stellar groups, we compared our data with different theoretical sets of isochrones over the CMDs and we also took into account the ST classifications (when available). We considered then two cases as follows.

(i) For brightest (earlier) stars, we compared their CMD position (see Fig. 6) with models computed for solar metallicity, mass-loss and overshooting (Marigo et al. 2008) shifted by adopted distance values for groups 'a' ($V_0 - M_V = 11.8$) and 'b' ($V_0 - M_V = 12.5$). Intrinsic scatter is present in our data and this fact prevents a unique isochrone solution; however, it is still possible to obtain an estimate of the age value for stellar groups 'a' and 'b', say ∼3 Myr. This value is consistent with the expected lifetime on the MS of the earlier stars of each group (∼O5). These values obtained for post-MS evolution were identified as 'nuclear ages'. For population 'c', we adopted the lifetime of an O9–B0 on MS (∼10 Myr) as age estimate.

(ii) For the faintest (PMS population) stars, we superimposed a set of the Siess et al. (2000) PMS models on CMDs presented in Fig. 5 using the respective $E(B - V)$ and $V_0 - M_V$ values. The transition from PMS to MS phase is also an extremely accurate age diagnostic. This phase is clearly seen in $R1$ and in $R3$, and to less extent in $R2$ and indicates an age between 2 and 3 Myr. The adopted age values for each group are indicated in Table 3 and are identified as 'contraction ages'.

Taking into account the uncertainties in the determinations of the ages and distances, it is possible to conclude that there is no significant difference between the more massive and less massive stars' ages.

3.6 PMS population

Regarding the PMS population, we noticed that most of X-ray sources are distributed uniformly inside $R1$ but tend to show uneven distributions between $R1$ and the regions $R2$ and $R3$, suggesting separated groups. On the other hand, identified YSOs are all placed in $R3$ (see Figs 1b and 5). This difference could be in part real and indicate a different evolutionary stage, but it is more conservatively caused by a distance objects population placed in this region as was suggested by the presence of a recently discovered embedded clusters using data from the deep near-infrared VVV[9] survey (Borissova et al. 2011).

In order to better understand the PMS population distribution in the region, we build the spatial density stellar maps selecting stars placed between the following limits: a PMS isochrone of 1 Myr (at $E(B - V) = 0.28$ and $V_0 - M_V = 11.8$) and a PMS isochrone of 5 Myr (at $E(B - V) = 0.37$ and $V_0 - M_V = 12.5$). In this process, we used first the triangles method (Kippenhahn, Weigert & Hofmeister 1967) for the selection over the CMDs of all the observed stars, and then we choose a spatial bin size of 1.0 arcmin and the drizzle method (Fruchter & Hook 2002) with a 15.0 arcsec step for the building of the density maps. Our results are presented in Fig. 8 where we distinguish stars brighter and fainter than $V = 17$ (∼1.6–2 $M_\odot$). We noticed that $V < 17$ stars (Fig. 8a) present overdensities well correlated with the previous selected regions according to the MS stars ($V < 12$). On the other hand, $V > 17$ stars (Fig. 8b) only presented an appreciable overdensity in the north part of $R1$. We also observed a close correlation between lower density regions in this plot and MSX sources – mainly located at south and east of $R1$–$R3$. This correlation indicates that this map mainly reflects the differential absorption present across our FOV and not real stellar concentrations.

All these facts reinforce the idea that the PMS population in the studied field is nearly 2 Myr, mainly concentrated in $R1$ and could be

[9] Vista Variables in the Via Lactea.

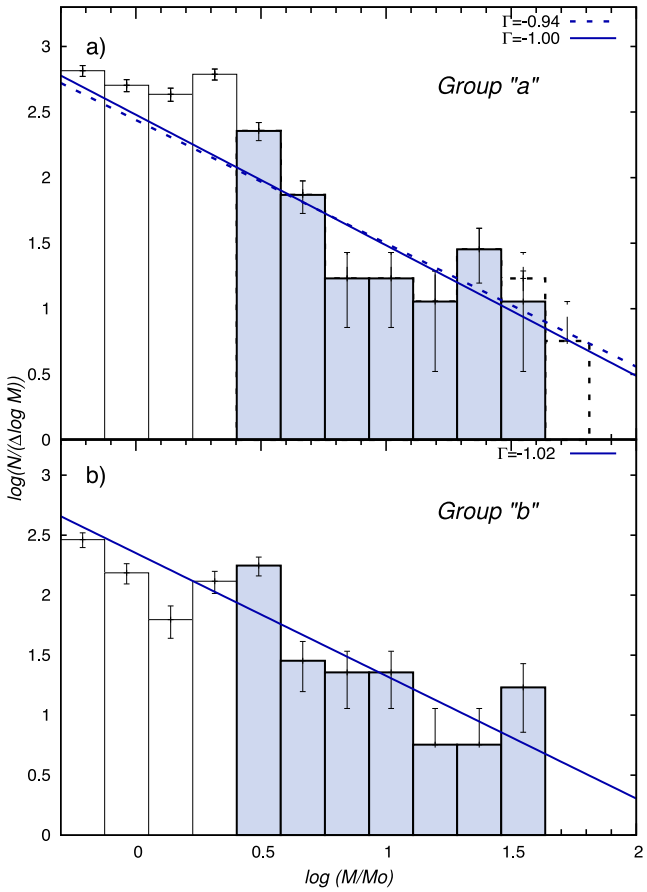

Figure 9. IMFs obtained for the stellar groups 'a' and 'b' (see Section 3.3). For group 'a', both cases represent results where HD 101205 was and was not included. Grey bins ($M > 2$ M$_\odot$) represent values considered to compute the power-law fits. Error bars indicate Poisson uncertainty.

revealed in our analysis up to $V = 17$. Fainter (less massive) possible PMS population could not be separated from the field population using this method.

3.7 The IMF of the main stellar group

The IMF can be approximated by a power law of form

$$\log\,(N/\Delta(\log m)) = \Gamma\,\log\,m,$$

where N is the number of star per logarithmic mass bin $\Delta(\log m)$.

We computed the IMFs for groups 'a' and 'b', using, respectively, stars located in regions $R1 + R2$ and $R3$ (see Section 3.3). To build the IMFs, we divided, on each region, the stars in two sets: brighter and fainter than $V = 12$. In the former case, we considered only stars adopted as members following our spectrophotometric analysis (see Section 3.2) and individual masses were estimated via a linear interpolation using the Marigo et al. (2008) model for 3 Myr. For the latter case, we considered the stars resulting from the statistical decontamination (see Section 3.2.2) and we used the Siess et al. (2000) stellar model for 3 Myr for deriving individual masses. We also considered the CFs (see Section 2.3) which, however, are important only at very low mass values ($M < 0.5$ M$_\odot$). Fig. 9 shows the resulting IMFs (histograms) and the least-squares fit to the data (lines). In all these fits, we took into account only stars with masses larger than 2 M$_\odot$. The IMF slopes are reported in Fig. 9 and Table 3. These values nicely compare (within the errors) with the Salpeter

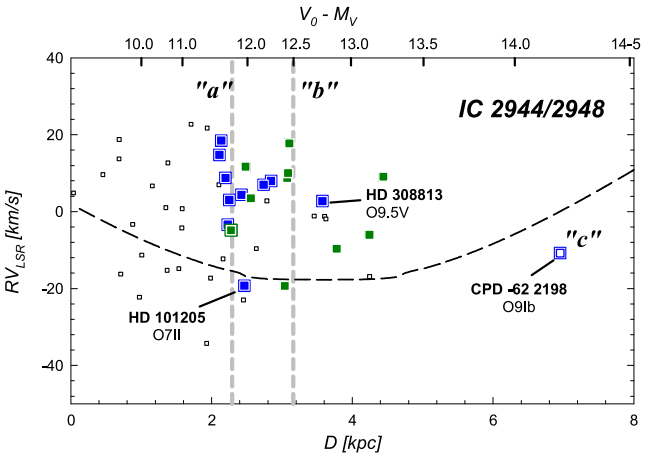

Figure 10. AL fit of the Galactic rotation model (dashed curve) applied to our Galaxy (Fich et al. 1989) and LSR radial velocities of stars placed in the studied zone (see Fig. 1). Symbols are of the same meaning as in Fig. 1(b). Vertical lines indicates the adopted 2.3 and 3.2 kpc distances ($V_0 - M_V = 11.8$ and $V_0 - M_V = 12.5$) for the stellar groups 'a' and 'b' (see Section 3.3).

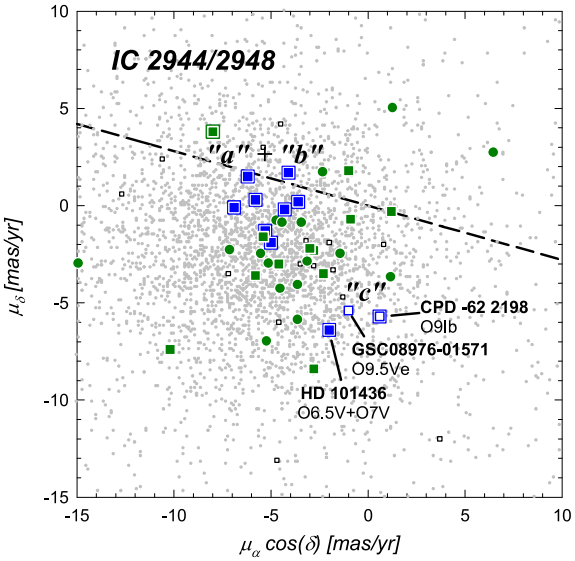

Figure 11. VPD for the stars brighter than $V = 16$. Symbols are of the same meaning as in Fig. 1(b). Dashed line indicates expected direction for movements parallel to the Galactic plane.

(1955) slope ($\Gamma = -1.35$), although they tend to be lower than this value.

We estimated the total mass of the stellar groups integrating over the mass range as follows: individual masses for all the stars with masses greater than 2 M$_\odot$ were summed up, while for lower masses, we estimated the amount of star at each mass bin using the values given by the power law. The estimated total masses for each stellar group are presented in Table 3.

We repeated the analysis, but using for the faint group only stars with an *XMM* counterpart. In this case, we obtained for each bin smaller numbers of sources (~15–30 per cent), as was expected from a simple visual inspection of Fig. 5. This difference might derive from X-ray data incompleteness and crowding, as previously suggested by Nazé et al. (2013). A similar situation was reported by Prisinzano et al. (2005) in their study of NGC 6530.

Table 4. Kinematic information for studied OB stars.

Name	RV_{LSR} (km s^{-1})		$N^{(*)}$	$\mu_\alpha \cos\delta$ (mas yr^{-1})		μ_δ (mas yr^{-1})		Binarity	RV source
HD 101205	−19	(20)		−6.2	(1.0)	1.5	(1.0)	SB2[b]	Kharchenko et al. (2007)
HD 101131	9	(11)	75	−5.8	(1.0)	0.3	(1.0)	SB2[a]	Gies et al. (2002)
HD 101190	8	(9)	20	−4.1	(1.0)	1.7	(1.0)	SB2[b]	Sana et al. (2011)
HD 101436	4	(10)	13	−2.0	(1.6)	−6.4	(4.2)	SB2[b]	Sana et al. (2011)
HD 101298	7	(8)	3	−3.6	(1.2)	0.2	(1.2)	SB?[b]	Thackeray & Wesselink (1965)
HD 101413	18	(16)	14	−6.9	(1.3)	−0.1	(1.4)	SB2[b]	Conti et al. (1977)
HD 101191	3	(7)	3	−6.9	(1.2)	−0.1	(1.2)	SB[b]	Thackeray & Wesselink (1965)
HD 101223	15	(7)	3	−5.0	(1.3)	−1.9	(1.7)	SB?[b]	Thackeray & Wesselink (1965)
HD 101333	−3	(5)	3	−5.3	(1.3)	−1.3	(1.3)	SB?[b]	Huang & Gies (2006)
HD 308813	3	(22)	3	−4.3	(1.4)	−0.2	(1.3)	SB[b]	Huang & Gies (2006)
HD 308818	9	(7)		−2.8	(5.1)	−2.3	(1.3)		Kharchenko et al. (2007)
CPD-62°2153	18	(7)		−2.3	(1.1)	−3.5	(1.3)		Kharchenko et al. (2007)
HD 308826	12	(–)		−3.0	(2.3)	−2.2	(2.0)		SIMBAD
HD 308825	−6	(0)	3	−4.6	(1.3)	−3.0	(3.1)		Huang & Gies (2006)
HD 308817	10	(9)	3	−10.2	(1.4)	−7.4	(1.6)		Huang & Gies (2006)
CPD-62°2198	−11	(4)	3	0.6	(1.1)	−5.7	(1.0)	SB?[b]	Huang & Gies (2006)
HD 308831	−19	(10)	3	−1.0	(3.1)	1.8	(3.5)		Huang & Gies (2006)
HD 308833	−10	(9)	3	1.2	(1.7)	−0.3	(2.4)		Huang & Gies (2006)
HD 308804	−5	(3)	3	−8.0	(1.5)	3.8	(2.6)	SB?[b]	Huang & Gies (2006)
HD 308832	9	(2)	3	−5.8	(1.8)	−3.6	(1.7)		Huang & Gies (2006)
GSC08976-00983	3	(7)	3	−0.9	(1.9)	−0.7	(1.7)		Huang & Gies (2006)

Notes.
(*) = Number of averaged spectra.
Errors are presented in parentheses.
Binarity source: [a]Gies et al. (2002); [b]Sana et al. (2011).
SB = Binary system, single spectra; SB2 = Binary system, double spectra; SB? = Dubious binary system (possible binary systems by Ardeberg & Maurice 1977 but probable single star by Sana et al. 2011).

3.8 Kinematic study

We extracted heliocentric radial velocities from the WEBDA data base for 25 stars (see Section 2.4). Since they come from different sources, taken at different epochs and with different spectral dispersions, we averaged the values obtained from better spectral resolution observations. For binary systems, their barycentric radial velocities were computed analysing the best-fitting curves from Gies et al. (2002) and Sana et al. (2011).

In order to compare the stellar radial velocities with a model of Galactic rotation, we corrected the heliocentric values to the local standard of rest (LSR). We adopted 13.3 km s^{-1} for the solar motion relative to the LSR – $(U, V, W)_\odot$ = (9.96, 5.25, 7.07) km s^{-1} – according to Aumer & Binney (2009) and we used the stellar spectrophotometric distances computed in Section 3.2.

As for the Galactic rotation curve, we considered the adjusted linear (AL) model and the power-law model (Fich, Blitz & Stark 1989). Since, in our case, both models provide similar results, we eventually chose the former. Results are presented in Fig. 10. We computed then the mean LSR velocities of the groups 'a' and 'b' considering only their O stars. In the case of the population 'c', only CPD-62°2198 star provided radial velocity data and it was adopted as a poor representative value for these stars (see Table 3). We then could conclude that stellar groups 'a' and 'b' (at about 2.3 and 3.2 kpc, respectively) do not follow the Galactic rotation model and it is possible that population 'c' could have a closer behaviour. We noticed that the particular kinematic behaviour in radial velocities of the studied stellar groups 'a' and 'b' could may have been mistakenly interpreted an individual member as a runaway star. In fact, it could be the case of star HD 101131, since this one was identified as a runaway object by van Buren, Noriega-Crespo & Dgani (1995). However, recently this star was only identified as an object with an associated extended source (Peri et al. 2012) with an excess 60 μm emission that could be produced by a bow shock (Noriega-Crespo, van Buren & Dgani 1997).

The cross-correlation of our photometric data against the UCAC4 catalogue allows us to analyse also the proper motion of more than 7500 stars in the studied area (see Fig. 1). Fig. 11 presents the vector point diagram (VPD), where we marked previously identified stars (as in Fig. 1b). Most of O stars considered that stellar groups 'a' or 'b' members show quite a similar motion. On the other hand, O stars identifying population 'c' (hollow blue symbols) seem to show again a different kinematic behaviour. We adopted then the averaged proper motions of O stars of each group as representative of each one and are presented in Table 3.

The kinematic information for brightest stars in the studied region was summarized in Table 4.

4 CONCLUSIONS

In this study, we reported on a deep optical photometric study of the region surrounding IC 2944/2948 at ($l \sim 294\overset{\circ}{.}8$; $b \sim -1\overset{\circ}{.}6$). Optical photometry was complemented with archival data, which include astrometry, shallow optical, IR and mid-IR photometry and spectroscopy. This region harbours a wealth of young stars, emission nebulae, compact dark clouds and probable YSOs. Out of this material, we could derive the main properties of different populations located in the area.

First, we could assess that there are several populations along this particular line of sight: we could describe a spreading population of B-type stars with an important range in distance, two stellar concentrations ('a' and 'b') located at ∼2.3 and ∼3.2 kpc, and

some early stars ('c') apparently representing a young population located as distant as 8 kpc.

Secondly, by focusing our attention on the main stellar concentrations, we revealed that they are hosting a relevant population of PMS stars and are as young as 2–3 Myr. We derived their IMFs and we found that their slope for massive stars is low but still compatible with the standard Salpeter law, and we also provided an estimate of each stellar group in $\sim$1100 and $\sim$500 $M_{\odot}$.

Thirdly, we found that all O stars in these two groups share similar kinematics and their representative values are different from that expected from Galactic rotation models in this part of the Milky Way. Regarding the mentioned young background population ('c'), we found that it could had an apparent different kinematics; we estimated an age of $\sim$10 Myr as a crude approximation.

Finally, we compared all these population's locations and characteristic with those results obtained at similar directions of the Galaxy and they are consistent with the idea of an almost tangent view along of the Sagittarius–Carina spiral arm. In particular, groups 'a' and 'b' would coincide with the near side of this arm, while group 'c' with the far side, and the spread of B stars is a continuous young population characteristic of a grand design spiral structure.

ACKNOWLEDGEMENTS

GB, MJR, MAC and JAP acknowledge support from CONICET (PIPs 112-201101-00301 and 112-201201-00226). The authors are much obliged for the use of the NASA Astrophysics Data System, of the SIMBAD data base and ALADIN tools (Centre de Données Stellaires – Strasbourg, France), and of the WEBDA open cluster data base. This publication also made use of data from: (a) the Two Micron All Sky Survey, which is a joint project of the University of Massachusetts and the Infrared Processing and Analysis Center/California Institute of Technology, funded by the National Aeronautics and Space Administration and the National Science Foundation; (b) the AAVSO Photometric All-Sky Survey (APASS), funded by the Robert Martin Ayers Sciences Fund; (c) the Midcourse Space Experiment (MSX). Processing of the data was funded by the Ballistic Missile Defense Organization with additional support from NASA Office of Space Science. We thank R. Martínez and H. Viturro for technical support. Finally, we thank the referee, whose comments helped to improve significantly the paper.

REFERENCES

Allen C. W., 1973, Astrophysical Quantities, 3rd edn. Athlone Press, London
Alter G., Balazs B., Ruprecht J., eds, 1970, Catalogue of Star Clusters and Associations, 2nd edn. Akad. Kiado, Budapest
Anderson E., Francis C., 2012, Astron. Lett., 38, 331
Ardeberg A., Maurice E., 1977, A&AS, 28, 153
Ardeberg A., Maurice E., 1980, A&AS, 39, 325
Ardeberg A., Maurice E., 1981, A&A, 98, 9
Aumer M., Binney J. J., 2009, MNRAS, 397, 1286
Baade D. et al., 1999, The Messenger, 95, 15
Baume G., Vázquez R. A., Carraro G., Feinstein A., 2003, A&A, 402, 549
Baume G., Carraro G., Momany Y., 2009, MNRAS, 398, 221
Baume G., Carraro G., Comeron F., de Elía G. C., 2011, A&A, 531, A73
Borissova J. et al., 2011, A&A, 532, A131
Carraro G., 2014, in Feltzing S., Zhao G., Walton N. A., Whitelock P. A., eds, Proc. IAU Symp. 298, Setting the Scene for Gaia and LAMOST. Cambridge Univ. Press, Cambridge, p. 7
Carraro G., Costa E., 2009, A&A, 493, 71
Conti P. S., Leep E. M., Lorre J. J., 1977, ApJ, 214, 759
Corti M. A., Orellana R. B., 2013, A&A, 553, A108
Corti M. A., Arnal E. M., Orellana R. B., 2012, A&A, 546, A62
Cousins A. W. J., 1978a, Mon. Notes Astron. Soc. South. Afr., 37, 62
Cousins A. W. J., 1978b, Mon. Notes Astron. Soc. South. Afr., 37, 77 (errata)
Egan M. P. et al., 2003, VizieR Online Data Catalog, 5114, 0
Feigelson E. D., Getman K. V., 2005, preprint (astro-ph/0501207)
Fich M., Blitz L., Stark A. A., 1989, ApJ, 342, 272
Fruchter A. S., Hook R. N., 2002, PASP, 114, 144
Gallart C. et al., 2003, AJ, 125, 742
Gies D. R., Penny L. R., Mayer P., Drechsel H., Lorenz R., 2002, ApJ, 574, 957
Henden A. A., Terrell D., Welch D., Smith T. C., 2010, BAAS, 42, 515
Hou L. G., Han J. L., Shi W. B., 2009, A&A, 499, 473
Huang W., Gies D. R., 2006, ApJ, 648, 580
Jester S. et al., 2005, AJ, 130, 873
Kenyon S. J., Hartmann L. W., 1990, ApJ, 349, 197
Kharchenko N. V., Roeser S., 2009, VizieR Online Data Catalog, 1280, 0
Kharchenko N. V., Scholz R.-D., Piskunov A. E., Röser S., Schilbach E., 2007, Astron. Nachr., 328, 889
Kippenhahn R., Weigert A., Hofmeister E. 1967, in Alder B., ed., Methods for Computational Physics: Vol. 7. Academic Press, New York, p. 129
Koornneef J., 1983, A&A, 128, 84
Lada C. J., Lada E. A., 2003, ARA&A, 41, 57
Lumsden S. L., Hoare M. G., Oudmaijer R. D., Richards D., 2002, MNRAS, 336, 621
McSwain M. V., Gies D. R., 2005, ApJS, 161, 118
Majaess D. J., Turner D. G., Lane D. J., 2009, MNRAS, 398, 263
Marigo P., Girardi L., Bressan A., Groenewegen M. A. T., Silva L., Granato G. L., 2008, A&A, 482, 883
Martins F., Plez B., 2006, A&A, 457, 637
Nazé Y., Rauw G., Sana H., Corcoran M. F., 2013, A&A, 555, A83
Noriega-Crespo A., van Buren D., Dgani R., 1997, AJ, 113, 780
Peri C. S., Benaglia P., Brookes D. P., Stevens I. R., Isequilla N. L., 2012, A&A, 538, A108
Perry C. L., Landolt A. U., 1986, AJ, 92, 844
Preibisch T., Zinnecker H., 1999, AJ, 117, 2381
Prisinzano L., Damiani F., Micela G., Sciortino S., 2005, A&A, 430, 941
Reipurth B., 2008, in Reipurth B., ed., ASP Monograph Publications, Vol. 5, Handbook of Star Forming Regions, Volume II: The Southern Sky. Astron. Soc. Pac., San Francisco, p. 213
Reipurth B., Corporon P., Olberg M., Tenorio-Tagle G., 1997, A&A, 327, 1185
Salpeter E. E., 1955, ApJ, 121, 161
Sana H., James G., Gosset E., 2011, MNRAS, 416, 817
Schmidt-Kaler Th., 1982, in Schaifers K., Voigt H. H., eds, Landolt-Börnstein: Numerical Data and Functional Relationships in Science and Technology. Springer-Verlag, Berlin, p. 14
Siess L., Dufour E., Forestini M., 2000, A&A, 358, 593
Skrutskie M. F. et al., 2006, AJ, 131, 1163
Sota A., Maíz Apellániz J., Morrell N. I., Barbá R. H., Walborn N. R., Gamen R. C., Arias J. I., Alfaro E. J., 2014, ApJS, 211, 10
Stetson P. B., 1987, PASP, 99, 191
Stetson P. B., 1992, in Bulter C. J., Elliot I., eds, IAU Colloq. 136: Stellar Photometry – Current Techniques and Future Developments. Cambridge Univ. Press, Cambridge, p. 291
Thackeray A. D., Wesselink A. J., 1965, MNRAS, 131, 121
Vallée J. P., 2008, AJ, 135, 1301
van Buren D., Noriega-Crespo A., Dgani R., 1995, AJ, 110, 2914
Vega E. I., Orsatti A. M., Marraco H. G., 1994, AJ, 108, 1834
Walborn N. R., 1972, AJ, 77, 312
Walborn N. R., 1987, AJ, 93, 868
Zacharias N., Finch C. T., Girard T. M., Henden A., Bartlett J. L., Monet D. G., Zacharias M. I., 2013, AJ, 145, 44

This paper has been typeset from a TEX/LATEX file prepared by the author.